



Hydrogenase Hot Paper

How to cite: *Angew. Chem. Int. Ed.* **2020**, 59, 16786–16794

International Edition: doi.org/10.1002/anie.202005208

German Edition: doi.org/10.1002/ange.202005208

Caught in the H_{inact} : Crystal Structure and Spectroscopy Reveal a Sulfur Bound to the Active Site of an O_2 -stable State of [FeFe] Hydrogenase

Patricia Rodríguez-Maciá⁺, Lisa M. Galle⁺, Ragnar Bjornsson⁺, Christian Lorent, Ingo Zebger, Yoshitaka Yoda, Stephen P. Cramer, Serena DeBeer,^{*} Ingrid Span,^{*} and James A. Birrell^{*}

Abstract: [FeFe] hydrogenases are the most active H_2 converting catalysts in nature, but their extreme oxygen sensitivity limits their use in technological applications. The [FeFe] hydrogenases from sulfate reducing bacteria can be purified in an O_2 -stable state called H_{inact} . To date, the structure and mechanism of formation of H_{inact} remain unknown. Our 1.65 Å crystal structure of this state reveals a sulfur ligand bound to the open coordination site. Furthermore, in-depth spectroscopic characterization by X-ray absorption spectroscopy (XAS), nuclear resonance vibrational spectroscopy (NRVS), resonance Raman (RR) spectroscopy and infrared (IR) spectroscopy, together with hybrid quantum mechanical and molecular mechanical (QM/MM) calculations, provide detailed chemical insight into the H_{inact} state and its mechanism of formation. This may facilitate the design of O_2 -stable hydrogenases and molecular catalysts.

Introduction

Hydrogen is a promising green energy carrier for the future because it can easily be produced by water electrolysis using renewable energy and, later used in a fuel cell to generate energy producing only water as a byproduct.^[1] Currently, H_2 is produced mostly from fossil fuels or to a small extent by water electrolysis using expensive noble metal catalysts. In nature, efficient and reversible H_2 conversion is performed by a group of metalloenzymes called hydrogenases.^[2] These biocatalysts use earth abundant metals such as nickel and/or iron in their active site.^[3] Of the three groups of

hydrogenases ([NiFe] hydrogenases, [FeFe] hydrogenases and [Fe] hydrogenases), the [FeFe] hydrogenases are the most active ($100\,000\text{ s}^{-1}$ in H_2 oxidation and up to $10\,000\text{ s}^{-1}$ in H^+ reduction).^[4] However, these enzymes are extremely oxygen sensitive.^[5] Vigorous efforts have been made in order to protect [FeFe] hydrogenases, and hydrogenases in general, from oxygen.^[6] Although various oxygen inactivation mechanisms have been proposed,^[7] there is still a lack of understanding on how exactly O_2 attacks their active site. Such insights may help in designing strategies to protect hydrogenases and molecular catalysts from O_2 damage.

The active site of the [FeFe] hydrogenases, the H-cluster, consists of a binuclear [2Fe] sub-cluster ($[2Fe]_{\text{H}}$) covalently attached by a cysteine sulfur to a [4Fe–4S] cluster ($[4Fe-4S]_{\text{H}}$).^[8] $[2Fe]_{\text{H}}$ contains two irons bridged by the thiol groups of an aza-propane 1,3-dithiolate (ADT) ligand,^[9] a bridging CO ligand, with an additional CN^- and CO ligated to each iron. The (proximal) iron (Fe_p) directly bound to the $[4Fe-4S]_{\text{H}}$ sub-cluster is always coordinatively saturated, while the distal iron (Fe_d) possesses an open coordination site in most catalytic states, where substrates (H_2 and H^+) and inhibitors (including CO and O_2) can bind. The nitrogen atom in the ADT bridge serves as a base and Fe_d acts as a Lewis acid, together forming a frustrated Lewis pair, which is essential to heterolytically split H_2 at Fe_d .^[3] The catalytic cycle of these enzymes has been extensively studied through different spectroscopic techniques.^[10]

When purified aerobically from the native organism, the [FeFe] hydrogenase from *Desulfovibrio desulfuricans* remains

[*] Dr. P. Rodríguez-Maciá,^[+] Dr. R. Bjornsson,^[+] Prof. Dr. S. DeBeer, Dr. J. A. Birrell
Department of Inorganic Spectroscopy, Max Planck Institute for Chemical Energy Conversion
Stiftstraße 34–36, 45470 Mülheim an der Ruhr (Germany)
E-mail: serena.debeer@cec.mpg.de
james.birrell@cec.mpg.de

Dr. P. Rodríguez-Maciá^[+]
Inorganic Chemistry Laboratory, Department of Chemistry, University of Oxford
South Parks Road, Oxford, OX1 3QR (UK)

Dr. L. M. Galle,^[+] Prof. Dr. I. Span
Physikalische Biologie, Heinrich-Heine-Universität Düsseldorf
Universitätsstraße 1, 40225 Düsseldorf (Germany)
E-mail: ingrid.span@hhu.de

C. Lorent, Dr. I. Zebger
Physikalische Chemie/ Biophysikalische Chemie, Institut für Chemie, Technische Universität Berlin
Straße des 17. Juni 135, 10623 Berlin (Germany)

Dr. Y. Yoda
Japanese Synchrotron Radiation Institute, Spring-8
1-1-1 Kouto, Mikazuki-cho, Sayo-gun, Hyogo 679-5198 (Japan)
Prof. Dr. S. P. Cramer
SETI Institute
189 Bernardo Avenue, Mountain View, California 94043 (USA)

[+] These authors contributed equally to this work.

Supporting information and the ORCID identification number(s) for the author(s) of this article can be found under:
<https://doi.org/10.1002/anie.202005208>.

© 2020 The Authors. Published by Wiley-VCH Verlag GmbH & Co. KGaA. This is an open access article under the terms of the Creative Commons Attribution License, which permits use, distribution and reproduction in any medium, provided the original work is properly cited.

in an inactive oxygen-stable state called H_{inact} (or $H_{\text{ox}}^{\text{air}}$), which can be reactivated upon reduction.^[4,11] This state is thought to be “overoxidized” with an $\text{Fe}^{\text{I}}\text{Fe}^{\text{II}}$ configuration at the binuclear site and an additional ligand bound to Fe_d .^[11] The reduction of H_{inact} to an intermediate state H_{trans} is reversible while the further conversion of H_{trans} to H_{ox} is thought to be irreversible, involving the release of the putative ligand from Fe_d .^[11] The nature of this putative ligand in the H_{inact} state has remained a mystery for more than two decades. Despite considerable spectroscopic analysis,^[12] new approaches are clearly needed to define the electronic and geometric configuration of the H-cluster, and identify the nature of the exogenous ligand. Theoretical calculations have suggested that the extra ligand could be H_2O or OH^- .^[13] Interestingly, an $[\text{FeFe}]$ hydrogenase from *Clostridium beijerinckii* has been shown to convert into the H_{inact} state in a highly reversible fashion, but the presence of an extra ligand bound in this state is so far unknown and its formation mechanism remains elusive.^[14]

Recently, we showed that the H_{inact} state is formed upon oxidation of *DdHydAB* in the presence of sulfide (Na_2S). Based on this result, we suggested that the extra ligand bound to the open coordination site might be a sulfur species, possibly SH^- .^[15] However, we were unable to identify whether sulfide was directly bound to the H-cluster, in what configuration, and whether there were any additional changes to the enzyme during H_{inact} formation. In this work, we identify the nature of the additional ligand as SH^- through combined crystallographic and spectroscopic investigations. These results together with hybrid QM/MM calculations provide deeper understanding on the formation mechanism of this state and how it is protected against O_2 . This new insight may allow the general protection of metalloenzymes against oxygen, enabling their implementation in fuel cells and ultimately, it may provide design principles for developing O_2 -stable bio-inspired molecular catalysts.

Results and Discussion

Crystal Structure of *DdHydAB* in the H_{inact} State

DdHydAB in the H_{inact} state was crystallized under aerobic conditions at 12°C . Brown crystals (indicating the presence of iron–sulfur clusters) were observed within three days and retained their dark color for at least two weeks. IR spectra of crystals taken from the same drop confirmed that the *DdHydAB* was in the H_{inact} state (Figure S1 in the Supporting Information). *DdHydAB* in the H_{inact} state crystallized in an orthorhombic space group $P2_12_12_1$, and the asymmetric unit contains one biological assembly. In contrast, the previously reported structure was obtained from crystals with the space group $P2_12_12_1$ and the asymmetric unit contained two biological assemblies. The structure of H_{inact} was solved using molecular replacement with the structure published by Nicolet et al.^[8b] (PDB ID 1HFE) as a starting model, and was refined to a resolution of 1.65 \AA (crystal parameters and refinement statistics in Table S1). The structure by Nicolet et al. is the only available structure of

DdHydAB and the redox state of the enzyme in these crystals was not defined but assumed to be a mixture of the H_{ox} and H_{red} states.

The overall architecture of *DdHydAB* in the H_{inact} state is essentially identical to the starting model with a root mean square deviation (RMSD) of 0.631 \AA (calculated for all $\text{C}\alpha$ atoms of residues 2–397 without outlier rejection, Figure 1 A). The electron density for the H-cluster in the active site is well-defined (Figure 2 A); however, the occupancy of the $[\text{2Fe}]$ sub-cluster had to be reduced to 0.6 to fit the experimental data. The low $[\text{2Fe}]$ content indicates the presence of some apo protein in the preparation, partly a limitation of the artificial maturation procedure (see methods in the Supporting Information),^[16] and partly from some decomposition of the H-cluster.^[15] A more detailed analysis of the atomic

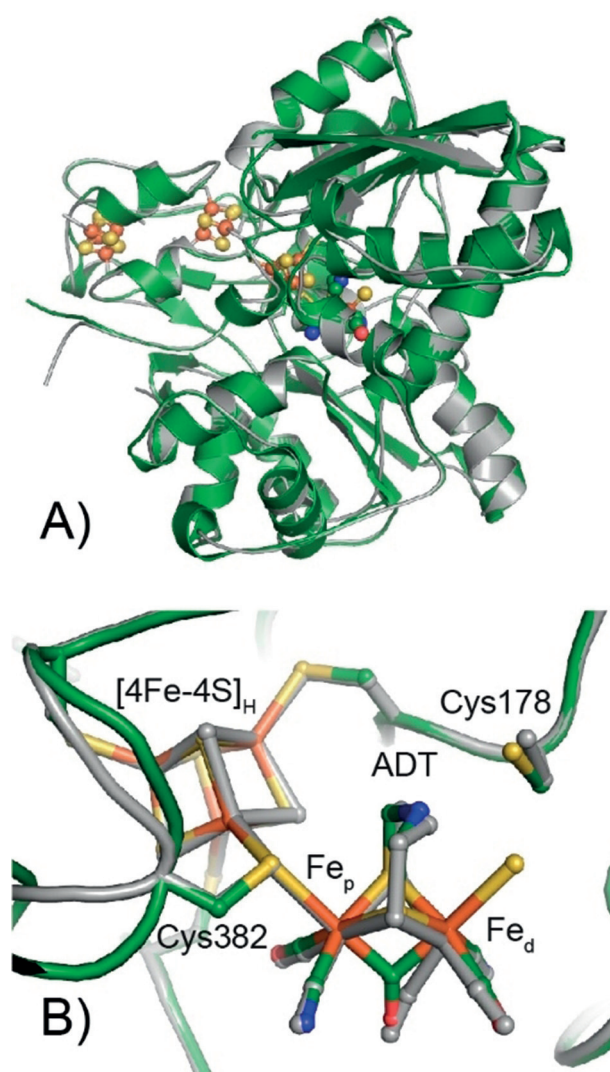


Figure 1. Superposition of the whole structure (A) and the active site H-cluster region (B) of *DdHydAB* in the H_{inact} state (green) and a partially reduced state from PDB ID 1HFE^[8b] (gray). The H-cluster, cluster ligating cysteines and C178 are shown in the sticks representation, and the protein backbone is shown in the cartoon representation. The overall architecture of *DdHydAB* in both states is virtually identical with an RMSD of 0.631 \AA (calculated for all $\text{C}\alpha$ atoms of residues 2–397).

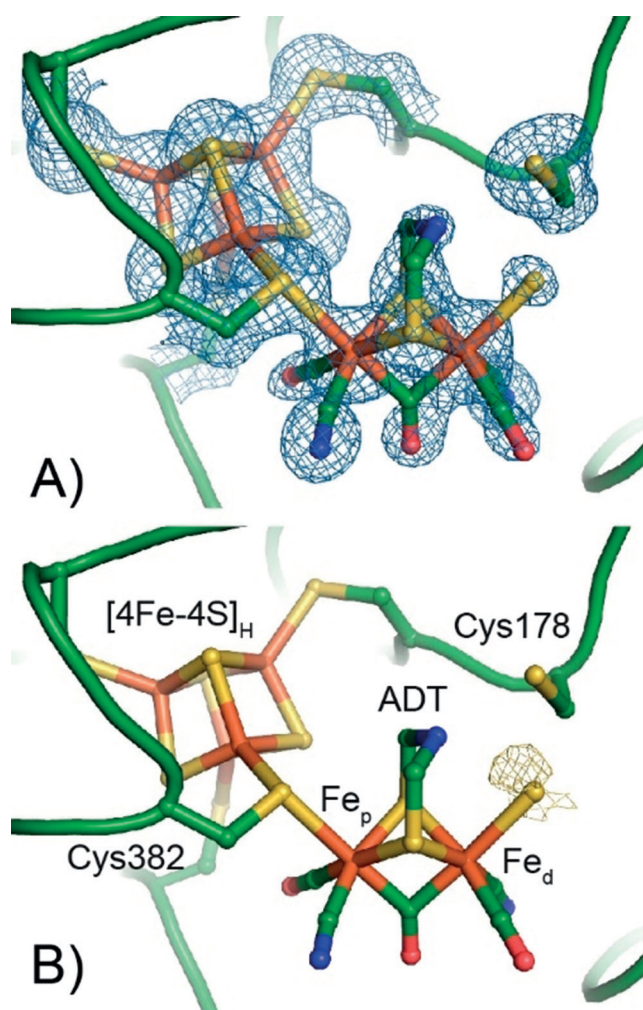


Figure 2. Crystal structure around the H-cluster in the H_{inact} state of DdHydAB. (A) The protein backbone is presented in the cartoon representation (green), and amino acid side chains and the H-cluster are shown in the stick representation. A $2Fo - Fc$ electron density map (blue mesh, contoured at 1.0σ) is shown for Cys178, all Cys ligating the $[4Fe-4S]_H$ sub-cluster and the H-cluster. An omit map generated from a model lacking the $[2Fe]_H$ sub-site and additional S ligand is shown in Figure S2. (B) Anomalous difference map (yellow mesh, contoured at 2.0σ) is shown for the additional ligand at the apical position on Fe_d .

coordinates at the $[2Fe]$ sub-site shows that there are a few small differences in the atomic positions, in particular at the bridging ligands, ADT and CO (Figure 1B), which likely, arise from the restraints introduced by the ligand library (crystallographic information file).^[17]

The more pronounced difference in the location and orientation of the bridging CO also arises from the different ligand restraints. While Nicolet et al. modelled the CO ligand as non-bonded; we used the ligand library also employed by Duan et al. for the $[FeFe]$ hydrogenase from *Clostridium pasteurianum* (CpHydA1).^[18] Notably, the temperature values of the bridging CO in our structure are lower than in the one reported by Nicolet et al., in agreement with our structure being that of a unique state, while Nicolet's structure was suggested to be a mixture of oxidized and reduced active

states.^[8b] No significant oxidative damage during crystallization or radiation damage to the accessory iron–sulfur clusters during the measurement were observed (Figure S3).

The electron density map reveals that the H-cluster is intact and contains two CN^- ligands, two terminal CO ligands, the bridging ADT ligand, as well as the bridging CO ligand (Figure 2A). In addition, the electron density in the active site clearly shows the presence of an additional ligand in the apical position on Fe_d at a distance of 2.4 \AA (see Figure S4). The ligand consists of only one non-hydrogen atom, in agreement with the presence of a (hydro)sulfide, hydroxide or oxo ligand. Modelling of the sulfur ligand with the same occupancy as that of the $[2Fe]$ subcluster (0.6) resulted in a good fit, but with a high B-factor (45 \AA^2), indicating some intrinsic disorder of the exogenous ligand. Modelling with an oxygen ligand gave a similar occupancy, but a slightly lower B-factor (38 \AA^2). Thus, anomalous scattering on exactly the same crystal was utilized to provide further information about the nature of the additional ligand. By measuring diffraction data at 6 keV , the anomalous signal from the iron atoms is suppressed, while that from other heavy atoms (such as S or Cl) is enhanced. The resulting anomalous electron density map shows clear evidence for anomalous density at the apical position on Fe_d (Figure 2B and Figure S5A and B). To further support this observation, anomalous diffraction measurements were also performed before native data collection on a second crystal obtained under identical conditions (see Supporting Information, Table S1). The anomalous density map of the second crystal also showed distinct anomalous density at the apical position on Fe_d . While this strongly supports that the additional ligand is actually a sulfur species, we cannot exclude the possibility of a Cl^- ligand. Interestingly, Cl^- has been suggested to bind to the H-cluster under certain circumstances.^[19] Hence, we investigated the spectroscopic properties of the H_{inact} state to provide further insight.

Characterization of the H_{inact} State by X-Ray Absorption Spectroscopy

X-ray absorption spectroscopy (XAS) on the H_{inact} state (containing the additional ligand) and the well-characterized H_{ox} state (lacking the additional ligand) were measured for comparison. Figure 3 shows the Fourier-transformed (FT) spectrum of the extended X-ray absorption fine structure (EXAFS) region for H_{ox} (Figure 3A) and H_{inact} (Figure 3B) after subtraction of the $[4Fe-4S]$ cluster contribution (see discussion in the Supporting Information). The presented data thus correspond to the average environment around the two iron atoms of the H-cluster. Comparison of the FTs clearly shows that the H-cluster of H_{inact} has greater amplitude than that of H_{ox} , consistent with the presence of an additional heavy scatterer in the first coordination sphere of H_{inact} . H_{ox} is best fit with 3 Fe–C scatterers at 1.80 \AA (from the terminal CN, terminal CO and the bridging CO), 2.5 Fe–S scatterers at 2.26 \AA (from ADT ligand sulfurs and the Fe_p -bound cysteine sulfur), and an Fe–Fe scattering path at 2.60 \AA (Table S4). In addition, Fe–C–O/N multiple scattering paths have to be included in the fit. The Fe–C–O/N multiple scattering paths

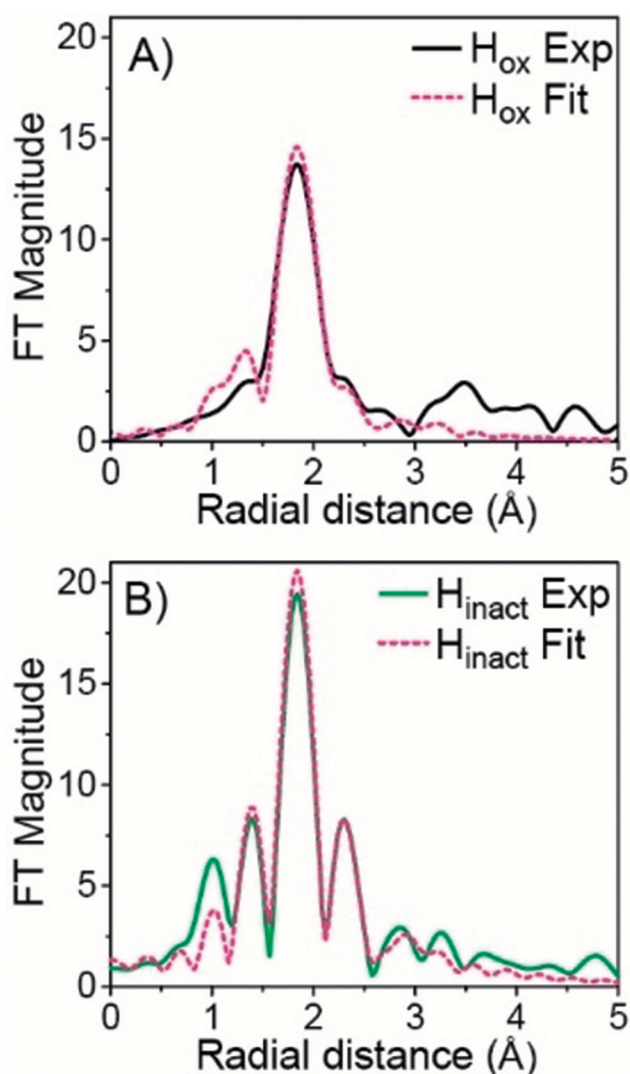


Figure 3. Non phase-shifted Fourier transform of k^3 -EXAFS of *DdHydAB* for H_{ox} (black solid line) and H_{inact} (green solid line). Corresponding fits shown as pink dashed lines. See Figure S12 for data before Fourier transformation and Table S4 and S5 for fitting parameters.

and the Fe–Fe scattering path are highly correlated, resulting in a somewhat larger error in the fit of the Fe–Fe distance.

For H_{inact} , the first shell consists of the same scattering paths (Fe–C, Fe–S, Fe–Fe and Fe–C–O multiple scattering) with the same degeneracy for every path as for H_{ox} except for the Fe–S path, for which the degeneracy needed to be increased to $N=3$ (see EXAFS Discussion and Table S5 in the Supporting Information). This is consistent with the presence of an additional S ligand in H_{inact} coordinated to one of the H-cluster Fe atoms. Attempts to separate the Fe–S contributions into shorter and longer Fe–S distances (as observed in the crystal structure) resulted in the fit paths coalescing to the same distance. This suggests that the separation of the two sulfur contributions is beyond the resolution of our data (≈ 0.16 Å). The ability to fit unique Fe–S contributions is further complicated by the strong correlation of the various scattering paths in our system.

Further, we note that similar to the protein crystallography, the EXAFS cannot distinguish between Cl or S as the additional ligand. Nevertheless, the first shell distances extracted from the EXAFS fits are in reasonable agreement, within the associated errors (≈ 0.1 Å), with the crystal structure (Table S5). For various crystal structures obtained with similar resolution diffraction data errors in the positions of the atoms, and hence bond lengths also, of up to 0.1 Å have been determined.^[20] Figure 4A presents the Fe K-edge XAS spectra of *DdHydAB* in the H_{ox} and H_{inact} states (with the [4Fe–4S] cluster contribution subtracted, see Supporting Information for details). The shift of the rising edge toward higher energy for H_{inact} is consistent with a more oxidized binuclear site (homovalent $Fe^{II}Fe^{II}$ in H_{inact} vs. mixed-valent $Fe^I Fe^{II}$ in H_{ox}). The differences in the pre-edge region (7110–7115 eV) suggest a different coordination environment of the [2Fe] sub-cluster in the two states.

To understand the features in the experimental XAS spectra and to gain insight into the origins of the observed

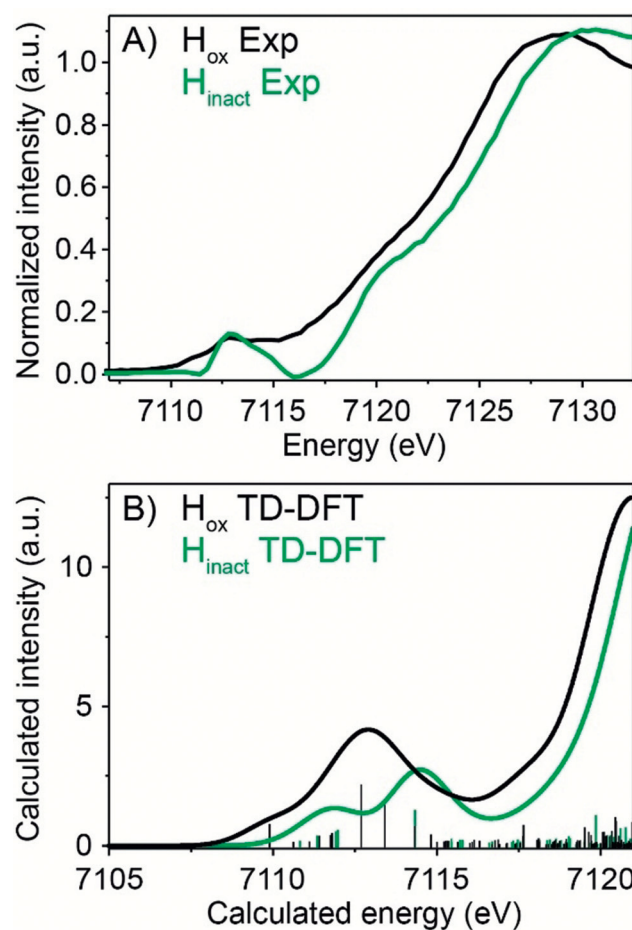


Figure 4. Fe K-edge XAS experimental and calculated spectra. Fe K-edge XAS spectra were measured in the partial fluorescence yield mode on 3 mm *DdHydAB* samples at 10 K. (A) Fe K-edge XAS difference spectra of *DdHydAB* H_{ox} (black trace) and H_{inact} (green trace) both apo subtracted. (B) TD-DFT calculated Fe K-edge XAS spectra using the QM/MM H_{ox} model (black trace) and the H_{inact} -SH model (green trace), applying a 2 eV (FWHM) broadening and an energy shift of 30.2 eV.

changes, time dependent density functional theory (TDDFT) calculations were performed with H_{ox} and H_{inact} -SH quantum mechanics/molecular mechanics (QM/MM) models (see Supporting Information Figure S7). The TDDFT calculated pre-edge spectra (Figure 4B) reproduce the general experimental trends in terms of the pre-edge energies, intensity distributions and the onset of the rising edge. This indicates that the QM/MM models are consistent with the XAS data. Overall, these results support an oxidized $Fe^{II}Fe^{II}$ sub-cluster for H_{inact} with a bound ligand at Fe_d . We note, however, that the XAS edges are not sensitive to the exact nature of the apical ligand (see Supporting Information).

Characterization of the H_{inact} State by Vibrational Spectroscopy

Figure 5 shows experimental and calculated IR spectra of the H_{ox} and H_{inact} states. In the experimental spectra, all the bands of H_{inact} are shifted toward higher energy with respect to H_{ox} . This is consistent with a more oxidized [2Fe] sub-cluster in H_{inact} , which leads to reduced backbonding into the π^* orbitals of the ligands resulting in shorter CO and CN bonds.^[21] The calculated IR spectra for the H_{ox} and H_{inact} -SH QM/MM models show that the calculated frequencies are in reasonable agreement (see Supporting Information for more details). The magnitudes of the shifts are underestimated, especially for the terminal CO groups, suggesting that the experimental change in back-bonding upon oxidation is not quite reproduced by the calculations (even though the H_{inact} -SH model is oxidized). Importantly, the calculated shift of the bridging CO, which should be sensitive to the addition of a new ligand is consistent with the experimental shift, albeit slightly underestimated as well.

Nuclear resonance vibrational spectroscopy (NRVS) measures vibrational sidebands coupled to nuclear transitions for Mössbauer-active nuclei, including ^{57}Fe .^[22] NRVS has already been used to study states of [FeFe] hydrogenases, including the catalytic intermediate H_{hyd} .^[23] Artificial maturation with ^{57}Fe -labelled [2Fe] precursors results in selectively labeled [^{57}Fe] sub-clusters.^[24] As such, predominantly vibrations associated with the [2Fe] sub-cluster are observed. Figure 6A presents the experimental NRVS spectra of H_{ox} and H_{inact} , where clear differences can be observed. Low energy features in the 150–400 cm^{-1} region emerge primarily from Fe–S vibrations (bending and stretching motions). Bands around 450 cm^{-1} are mostly due to Fe–CN motion, while the strong bands between 500–600 cm^{-1} arise predominantly from Fe–CO bending and stretching modes. By correlating the experimental spectra to QM/MM NRVS calculations, the most important differences in the spectra can be interpreted. The calculated NRVS spectra (B) using the H_{ox} and H_{inact} -SH models correlate well with the experimental. Plots C and D in Figure 6 highlight the Fe–S region of the NRVS spectra. Compelling evidence for an extra sulfur bound to H_{inact} arise from the peak at $\approx 350\text{ cm}^{-1}$ (356.52 cm^{-1} in the calculated spectrum) in the Fe–S region (marked with an asterisk). We note that the absolute prediction of complete NRVS spectra from theoretical calculations is a challenge due to the densely populated

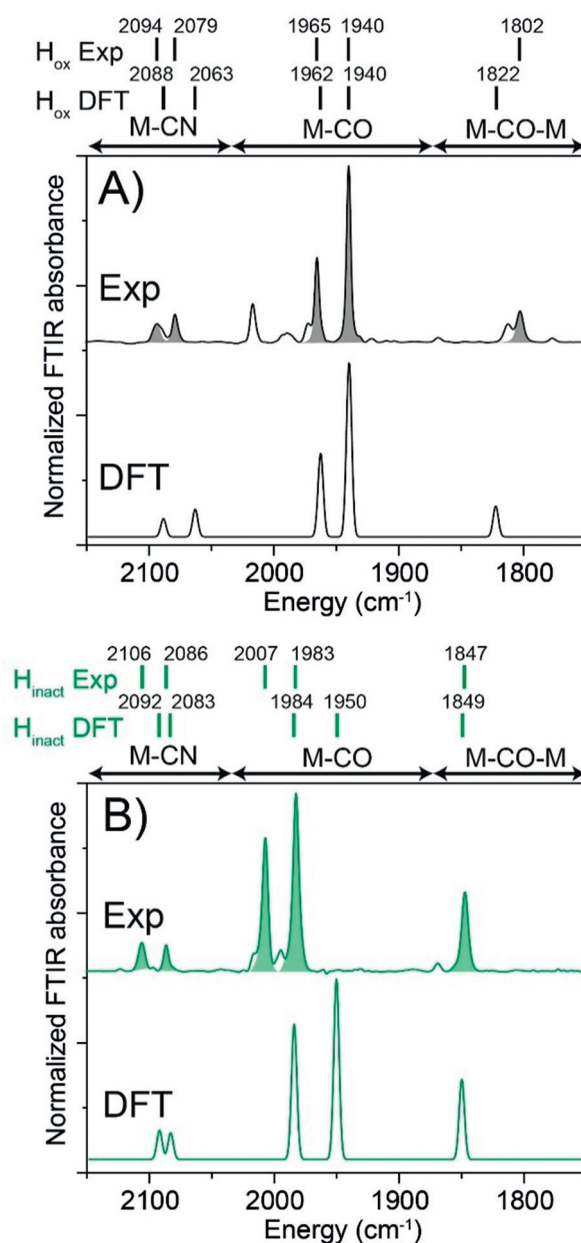


Figure 5. Experimental (above) and calculated (below) IR spectra of *DdHydAB* in (A) the H_{ox} state and (B) the H_{inact} state. The experimental IR spectra were measured at 25 °C and 2 cm^{-1} resolution. For the calculated IR spectra, the QM/MM H_{ox} and H_{inact} -SH models were used. The experimental intensities were used in the plotted DFT spectra. Scaling factors for calculated frequencies were used (see Supporting Information).

spectra and the nature of the low-energy modes involved, which are sensitive to the computational model. It is, therefore, advantageous to focus on the difference between H_{ox} and H_{inact} and on the Fe–S region.

Calculations reveal that the increased intensity in this region of the H_{inact} -SH model (compared to H_{ox}) arises from the Fe–S stretching vibration associated with an SH ligand. This feature is reproduced by the H_{inact} -SH model but cannot be reproduced in models with lighter ligands such as OH^- (see Supporting Information, Figure S23). The calculations cannot

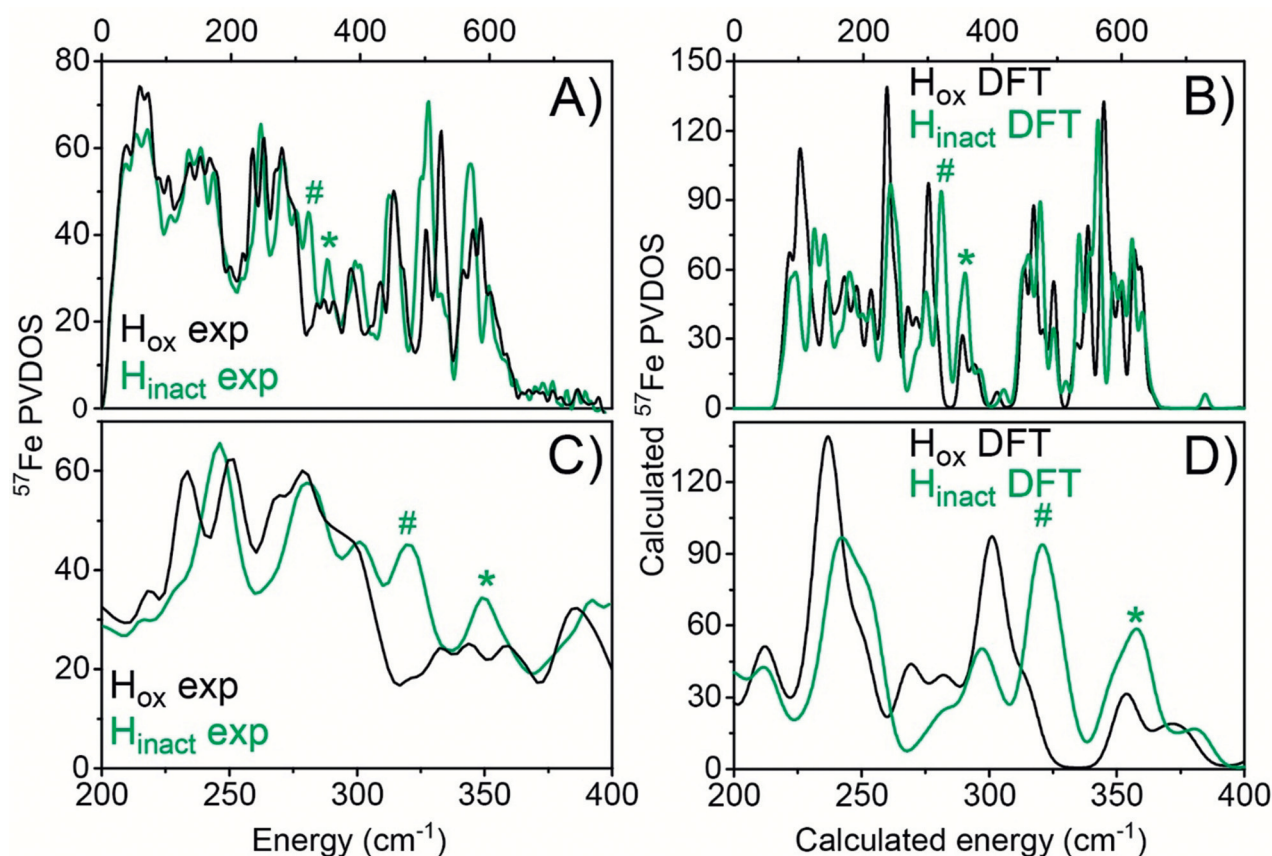


Figure 6. Experimental and calculated NRVS data of *DdHydAB* in the H_{ox} and H_{inact} states. The spectra were measured on 3 mm *DdHydAB* samples at 40–70 K. (A) Experimental NRVS data of H_{ox} (black trace) and H_{inact} (green trace). (B) Calculated NRVS data using the H_{ox} QM/MM model (black trace) and the H_{inact} -SH QM/MM model (green trace). C and D are enlargements of the Fe–S vibrational region of A and B, respectively. The asterisk indicates the peak assigned primarily to a terminal –SH group in H_{inact} while the hashtag indicates other Fe–S modes (associated with ADT ligand and Fe_p -Cys) that shift upon oxidation.

exclude a Cl^- ligand bound to Fe_d due to its similar mass and covalency, which gives a comparable spectrum in this region (see Supporting Information, Figure S23). However, the H_{inact} state can be formed in the strict absence of chloride (Figure S20), suggesting that a Cl^- bound to the open coordination site is unlikely. Furthermore, the experimental peak at $\approx 322\text{ cm}^{-1}$ (324 cm^{-1} in the calculated spectra) in H_{inact} (marked with a hashtag) is assigned to Fe–S modes from the ADT ligand and cysteine, which are shifted to higher energy (compared to H_{ox}) due to a more oxidized [2Fe] sub-cluster. The calculations demonstrate the sensitivity of NRVS spectra with respect to cluster oxidation state, but also with respect to the light vs. heavy atom nature of the ligand.

In order to directly identify the exogenous sulfur ligand, we compared NRVS spectra of H_{inact} samples prepared using natural abundance (95% ^{32}S) and ^{34}S -labelled sodium sulfide. We observed small differences between the ^{32}S and ^{34}S spectra, particularly in the $340\text{--}360\text{ cm}^{-1}$ region (Figure 7B and Figure S24). Similar results were obtained with resonance Raman (RR) spectroscopy (Figure 7A and Figure S25), where small changes can be observed in the $340\text{--}360\text{ cm}^{-1}$ region when going from the ^{32}S spectrum to the ^{34}S spectrum, coinciding with the expected lower frequencies of vibrations related to a heavier atom. Calculations support the assign-

ment of two peaks in this region to Fe–S stretching modes from exogenously bound SH^- (Figure 7C and Table S12).

Mechanism of H_{inact} Formation and Implications

Using our QM/MM model, we calculated the binding of H_2S to the H_{ox} state, (see Scheme in Figure S26).^[15] Sulfur likely reaches the H-cluster via diffusion through the same hydrophobic gas channels used by H_2 , CO and O_2 . Thus, protonation to H_2S ($pK_a \approx 7$)^[25] in solution facilitates this process. Interestingly, partial formation of a very similar H_{inact} state with Na_2Se could be achieved (Figure S27), but only at pH 4, where the enzyme is not very stable. This supports the idea that the neutral species (H_2S or H_2Se) are involved, as H_2Se has a much lower pK_a (3.89)^[25] than H_2S . Direct H_2S binding to H_{ox} is calculated to be thermoneutral ($\Delta G = +0.2\text{ kcal mol}^{-1}$), while deprotonation of bound H_2S by the NH group of the ADT is quite favorable ($\Delta G = -4.9\text{ kcal mol}^{-1}$). This leads to an Fe–SH bound intermediate that is favorable with respect to free H_2S ($\Delta G = -4.7\text{ kcal mol}^{-1}$). The H-cluster is subsequently oxidized to give an $Fe^{II}Fe^{III}$ binuclear sub-cluster, a process driven by application of oxidizing potentials. This likely proceeds via proton-coupled

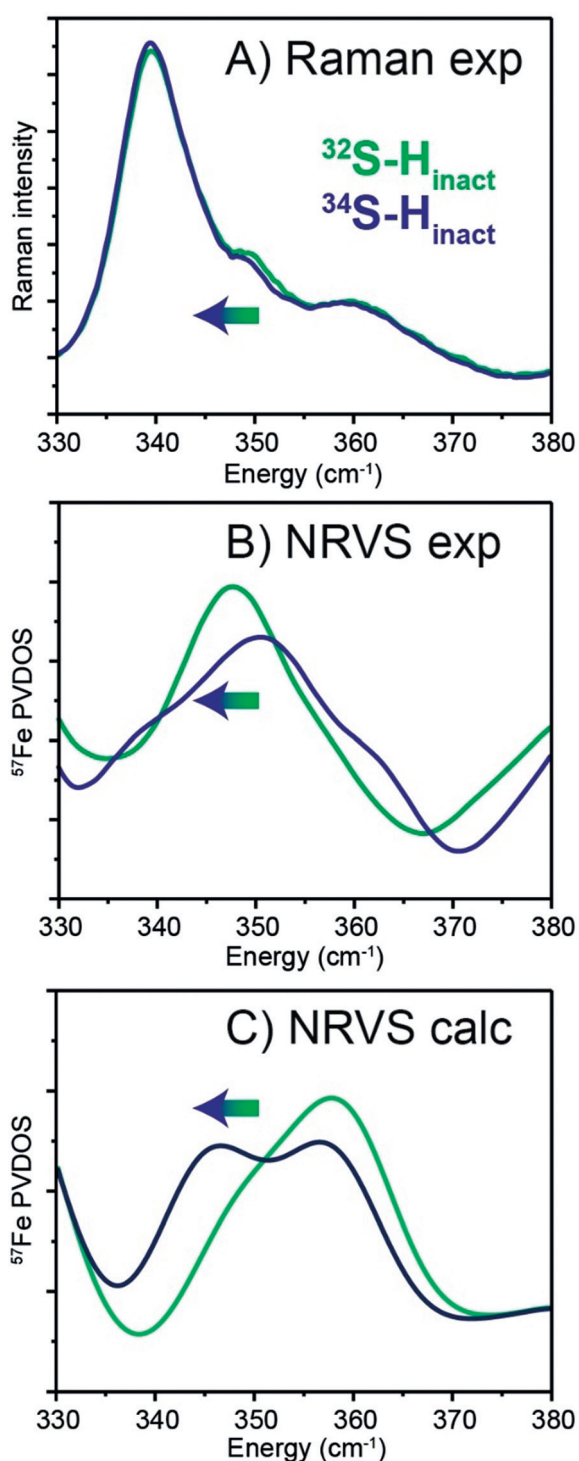


Figure 7. ³²S/³⁴S isotope related shifts in the vibrational spectra of the H_{inact} state. A) Resonance Raman spectra were measured on 3 mm *DdHydAB* samples at 80 K using 514 nm excitation. Experimental spectra of H_{inact} prepared with natural abundance Na₂S (green trace) and ³⁴S-labelled Na₂S (blue) in the Fe–S region between 330 and 380 cm⁻¹ (see Figure S25 for the full spectrum). The spectra are normalized to modes at 622 cm⁻¹ and 644 cm⁻¹ corresponding to the amino acid side chains phenylalanine and tyrosine, respectively.^[30] Experimental (B) and QM/MM-calculated ⁵⁷Fe NRVS data (C) The corresponding spectra of *DdHydAB* in the H_{inact} state with ³²S (green) and ³⁴S (blue) ligand are also displayed in the region between 330 and 380 cm⁻¹ (see Figure S24 for the full spectra and a wider view of the Fe–S region). Calculated band positions using the H_{inact}-SH QM/MM model with ³²S and ³⁴S bound at open coordination site of Fe_d are presented in Table S12 and shown as Movies S1 and S2.

A number of other metalloenzymes bind sulfide under similar conditions. Both [NiFe] hydrogenase and Ni-dependent CO dehydrogenase are inhibited by sulfide at high applied potentials, presumably by sulfide binding in a bridging position between Ni and Fe.^[26] Recent studies suggest that, in nitrogenase, reductive displacement of an active site “belt” sulfide could be important for binding of substrates/inhibitors.^[27] Thus, binding of additional sulfides to compensate for increased positive charge on oxidized metal ions could be a common theme among enzymes, highlighting the importance of understanding how sulfide interacts with metals in nature. Diiron model complexes including thioether groups are also involved in oxidation state dependent sulfur coordination from the S group.^[28] However, in none of these cases has additional oxygen protection due to sulfur binding been demonstrated, as is observed in [FeFe] hydrogenase.

Handling air-sensitive enzymes such as [FeFe] hydrogenases under air has definite advantages, particularly, for crystallization and manipulation of crystals. Our *DdHydAB* H_{inact} structure is the first [FeFe] hydrogenase structure for which the redox state has been defined using single crystal spectroscopy, as previously demonstrated for [NiFe] hydrogenases.^[29] This provides the opportunity to directly correlate structural and spectroscopic properties of the H-cluster. Interestingly, there are very few differences in the structure of the H-cluster compared with previously published structures, suggesting an H-cluster environment that minimizes redox state dependent structural changes, lowering reorganization energy and enhancing catalysis. Air-stable [FeFe] hydrogenases may also be industrially useful for example, in fuel cells. Fuel cells containing [FeFe] hydrogenase embedded in a redox polymer have been prepared under strict anaerobic conditions,^[6] but could be prepared under air with the H_{inact} state, simplifying the process and increasing the scalability.

electronic rearrangement, whereby the electron is first transferred from the binuclear sub-cluster to the [4Fe–4S] sub-cluster, followed by its oxidation. The oxidation steps take place by one-electron transfers from the [4Fe–4S]_H subcluster, via the F-clusters, to the available high potential oxidant (including oxygen). Calculations performed with our H_{inact}-OH QM/MM model suggest that H₂O binds effectively at H_{ox} but will not deprotonate via the ADT ligand, due to the larger pK_a difference than for H₂S (see Supporting Information).

The Relevance of O₂ Protection via H_{inact} In Vivo

The bacterium *Desulfovibrio desulfuricans* has evolved in anaerobic environments and, therefore, its hydrogenase is extremely oxygen sensitive, becoming inactivated irreversibly even by traces of O₂.^[11,31] Although the mechanism of oxygen inactivation is not yet completely understood, O₂ is believed to attack the active site by binding to the open coordination

site on Fe_d .^[30] If the bound- O_2 cannot be reduced to water, it may form reactive oxygen species, which could destroy the active site. As the open coordination site is blocked by sulfide in the H_{inact} state, this prevents O_2 binding and destruction of the active site.

A plausible scenario is that in vivo, *DdHydAB* is constantly exposed to H_2S (since *Desulfovibrio desulfuricans* reduces sulfate to sulfide). Under reductive conditions H_2S is displaced by H_2 , binding to the H-cluster. In the presence of oxygen, however, H_2S becomes locked to the H-cluster forming the H_{inact} state to protect the enzyme from oxygen inactivation. It is interesting that the [FeFe] hydrogenase from *Clostridium beijerinckii* (*CbH5A*) can form the H_{inact} state without exogenous sulfide.^[14] How, the H_{inact} state in this enzyme differs structurally from that in *DdHydAB* is not known, but it seems likely that, in the absence of available sulfide in this organism, an endogenous sulfur ligand, such as a cysteine nearby the active site, has evolved to play a role. Another important difference between these two enzymes is that *DdHydAB* functions as a periplasmic H_2 uptake enzyme with extremely high activity,^[32] while *CbH5A* shows a strong bias for H_2 production.^[14] This lack of activity in H_2 uptake may be due to spontaneous formation of H_{inact} at high potentials. As *DdHydAB* requires exogenous sulfide, it will only be inactive when sulfide levels are high, which may serve to regulate metabolism.

Conclusion

Here, we provide direct structural and spectroscopic evidence for an exogenously bound sulfur in the apical coordination site of the [FeFe] hydrogenase from *Desulfovibrio desulfuricans* in the O_2 -stable H_{inact} state. In our previous work, we showed that exogenous sulfide was required for H_{inact} formation, but we were unable to demonstrate if and how sulfide binds to the H-cluster. The 1.65 Å crystal structure shows electron density at the apical position on the distal Fe and anomalous diffraction suggests this is consistent with sulfur. EXAFS shows an additional sulfur in the Fe-coordination environment of H_{inact} compared with H_{ox} . Fe K-edge XAS data reveal a more oxidized [2Fe] sub-cluster in H_{inact} compared to H_{ox} and a different coordination environment of the Fe ions in the [2Fe] subcluster. Comparison of H_{inact} and H_{ox} NRVS spectra, as well as $^{32}\text{S}/^{34}\text{S}$ isotope labelling in both NRVS and resonance Raman spectroscopy, provide additional compelling evidence for an exogenous sulfur ligand. Calculations with an $\text{H}_{\text{inact}}\text{-SH}$ model provide close agreement to all the experimental data and shed light on the mechanism of forming H_{inact} . In particular, the most likely pathway involved H_2S binding at the open coordination site, followed by proton transfer via the ADT ligand to the proton transfer channel. H_{inact} formation is then completed upon proton coupled electronic reconfiguration of the H-cluster and oxidation of $[\text{4Fe-4S}]_{\text{H}}$. Since we previously demonstrated that this in vitro H_{inact} approach works for other [FeFe] hydrogenases such as *Chlamydomonas reinhardtii* (*CrHydA1*), it demonstrates the wider applicability of this method. Thus, it would be interesting to perform similar structural and

spectroscopic studies of H_{inact} in other enzymes, including *CbH5A* and *CrHydA1*. Our highly complementary structural, spectroscopic and theoretical approach represents a major advance for the understanding the function of this O_2 -stable state and its mechanism of formation, as well as a possible implementation of these enzymes in biotechnological applications.

Acknowledgements

The authors would like to thank Nina Breuer and Patricia Malkowski for help with preparation of *DdHydAB* samples. Dr. George E. Cutsail III, Dr. Justin Travis Henthorn, Dr. Alexander Gutt and Dr. Casey Van Stappen are gratefully thanked for helpful assistance with X-ray data collection and for fruitful discussions. Dr. Justin Travis Henthorn and Ms. Rebeca G. Castillo are also thanked for helping to prepare the Na_2^{34}S and to fit the pre-edge region for H_{ox} and H_{inact} , respectively. We acknowledge Dr. Casey Van Stappen for his help in preparing XAS plots. We are also grateful to Dr. Erik Jonathan Nelson and Dr. Matthew J. Latimer at SSRL for providing assistance in using beamline 9-3 and to Dr. Kenji Tamasaku for assistance in NRVS measurements in Spring-8. We acknowledge DESY (Hamburg, Germany), a member of the Helmholtz Association HGF, for the provision of experimental facilities. Parts of this research were carried out at PETRA III and we would like to thank Anja Burkhardt, Olga Lorbeer, and Eva Crosas for assistance in using the Bioimaging and diffraction beamline P11. The authors would also like to express their gratitude to Dr. Nipa Chongdar for critical reading of the manuscript. $(\text{Et}_4\text{N})_2\text{-}[\text{Fe}_2(\text{ADT})(\text{CO})_4(\text{CN})_2]$ was a kind gift from Prof. Thomas B. Rauchfuss, University of Illinois Urbana-Champaign, IL, USA. NRVS data were collected during beam times 2018B1379 and 2019A1259 at BL19LXU at SPring-8, Japan. This work was financially supported by the Max Planck Society (P.R.-M., S.D., J.A.B.), the Deutsche Forschungsgemeinschaft (DFG) Priority Programme “Iron-Sulfur for Life: Cooperative Function of Iron-Sulfur Centers in Assembly, Biosynthesis, Catalysis and Disease” (SPP 1927) Projects DE 1877/1-1 (S.D.), BI 2198/1-1 (J.A.B.), IS 1476/4-1 (I.S.) and ZE 510/2-2 (I.Z., C.L.); further funded by the Deutsche Forschungsgemeinschaft (DFG, German Research Foundation) under Germany’s Excellence Strategy—EXC 2008–390540038—UniSysCat (I.Z., C.L.), and the National Institutes of Health NIH GM-65440 (S.P.C.). S.P.C. and I.Z. are grateful to the Einstein Foundation Berlin for funding (grant number EVF-2016-277). Use of the Stanford Synchrotron Radiation Lightsource, SLAC National Accelerator Laboratory, is supported by the U.S. Department of Energy (DOE), Office of Science, Office of Basic Energy Sciences under Contract No. DE-AC02-76SF00515. The SSRL Structural Molecular Biology Program is supported by the DOE Office of Biological and Environmental Research, and by the National Institutes of Health, National Institute of General Medical Sciences (including P41GM103393). Open access funding enabled and organized by Projekt DEAL.

Conflict of interest

The authors declare no conflict of interest.

Keywords: hydrogenase · protein structures · sulfide · vibrational spectroscopy · x-ray absorption spectroscopy

-
- [1] N. Armaroli, V. Balzani, *ChemSusChem* **2011**, *4*, 21–36.
- [2] K. A. Vincent, A. Parkin, F. A. Armstrong, *Chem. Rev.* **2007**, *107*, 4366–4413.
- [3] W. Lubitz, H. Ogata, O. Rüdiger, E. Reijerse, *Chem. Rev.* **2014**, *114*, 4081–4148.
- [4] W. G. Martin, B. R. Glick, S. M. Martin, *Can. J. Microbiol.* **1980**, *26*, 1214–1223.
- [5] F. A. Armstrong, J. Hirst, *Proc. Natl. Acad. Sci. USA* **2011**, *108*, 14049–14054.
- [6] A. A. Oughli, F. Conzuelo, M. Winkler, T. Happe, W. Lubitz, W. Schuhmann, O. Rüdiger, N. Plumeré, *Angew. Chem. Int. Ed.* **2015**, *54*, 12329–12333; *Angew. Chem.* **2015**, *127*, 12506–12510.
- [7] a) S. T. Stripp, G. Goldet, C. Brandmayr, O. Sanganas, K. A. Vincent, M. Haumann, F. A. Armstrong, T. Happe, *Proc. Natl. Acad. Sci. USA* **2009**, *106*, 17331–17336; b) K. D. Swanson, M. W. Ratzloff, D. W. Mulder, J. H. Artz, S. Ghose, A. Hoffman, S. White, O. A. Zadornyy, J. B. Broderick, B. Bothner, P. W. King, J. W. Peters, *J. Am. Chem. Soc.* **2015**, *137*, 1809–1816; c) A. Kubas, C. Orain, D. De Sancho, L. Saujet, M. Sensi, C. Gauquelin, I. Meynial-Salles, P. Soucaille, H. Bottin, C. Baffert, V. Fourmond, R. B. Best, J. Blumberger, C. Léger, *Nat. Chem.* **2017**, *9*, 88–95.
- [8] a) J. W. Peters, W. N. Lanzilotta, B. J. Lemon, L. C. Seefeldt, *Science* **1998**, *282*, 1853–1858; b) Y. Nicolet, C. Piras, P. Legrand, C. E. Hatchikian, J. C. Fontecilla-Camps, *Structure* **1999**, *7*, 13–23.
- [9] A. Silakov, B. Wenk, E. Reijerse, W. Lubitz, *Phys. Chem. Chem. Phys.* **2009**, *11*, 6592–6599.
- [10] a) A. Adamska, A. Silakov, C. Lambertz, O. Rüdiger, T. Happe, E. Reijerse, W. Lubitz, *Angew. Chem. Int. Ed.* **2012**, *51*, 11458–11462; *Angew. Chem.* **2012**, *124*, 11624–11629; b) C. Sommer, A. Adamska-Venkatesh, K. Pawlak, J. A. Birrell, O. Rüdiger, E. J. Reijerse, W. Lubitz, *J. Am. Chem. Soc.* **2017**, *139*, 1440–1443; c) D. W. Mulder, Y. Guo, M. W. Ratzloff, P. W. King, *J. Am. Chem. Soc.* **2017**, *139*, 83–86; d) S. Katz, J. Noth, M. Horch, H. S. Shafaat, T. Happe, P. Hildebrandt, I. Zebger, *Chem. Sci.* **2016**, *7*, 6746–6752.
- [11] W. Roseboom, A. L. de Lacey, V. M. Fernández, C. Hatchikian, S. P. J. Albracht, *J. Biol. Inorg. Chem.* **2006**, *11*, 102–118.
- [12] A. S. Pereira, P. Tavares, I. Moura, J. J. G. Moura, B. H. Huynh, *J. Am. Chem. Soc.* **2001**, *123*, 2771–2782.
- [13] C. Greco, M. Bruschi, L. De Gioia, U. Ryde, *Inorg. Chem.* **2007**, *46*, 5911–5921.
- [14] S. Morra, M. Arizzi, F. Valetti, G. Gilardi, *Biochemistry* **2016**, *55*, 5897–5900.
- [15] P. Rodríguez-Maciá, E. J. Reijerse, M. van Gastel, S. DeBeer, W. Lubitz, O. Rüdiger, J. A. Birrell, *J. Am. Chem. Soc.* **2018**, *140*, 9346–9350.
- [16] J. A. Birrell, K. Wrede, K. Pawlak, P. Rodríguez-Maciá, O. Rüdiger, E. J. Reijerse, W. Lubitz, *Isr. J. Chem.* **2016**, *56*, 852–863.
- [17] a) I. D. Brown, B. McMahon, *Acta Crystallogr. Sect. B* **2002**, *58*, 317–324; b) S. R. Hall, F. H. Allen, I. D. Brown, *Acta Crystallogr. Sect. A* **1991**, *47*, 655–685.
- [18] J. Duan, M. Senger, J. Esselborn, V. Engelbrecht, F. Wittkamp, U.-P. Apfel, E. Hofmann, S. T. Stripp, T. Happe, M. Winkler, *Nat. Commun.* **2018**, *9*, 4726.
- [19] M. del Barrio, M. Sensi, L. Fradale, M. Bruschi, C. Greco, L. de Gioia, L. Bertini, V. Fourmond, C. Léger, *J. Am. Chem. Soc.* **2018**, *140*, 5485–5492.
- [20] a) J. M. Guss, H. D. Bartunik, H. C. Freeman, *Acta Crystallogr. Sect. B* **1992**, *48*, 790–811; b) E. I. Solomon, R. K. Szilagy, S. DeBeer George, L. Basumallick, *Chem. Rev.* **2004**, *104*, 419–458.
- [21] a) J. F. Siebel, A. Adamska-Venkatesh, K. Weber, S. Rumpel, E. Reijerse, W. Lubitz, *Biochemistry* **2015**, *54*, 1474–1483; b) P. Rodríguez-Maciá, E. Reijerse, W. Lubitz, J. A. Birrell, O. Rüdiger, *J. Phys. Chem. Lett.* **2017**, *8*, 3834–3839.
- [22] H. Wang, E. E. Alp, Y. Yoda, S. P. Cramer, in *Metalloproteins: Methods and Protocols* (Eds.: J. C. Fontecilla-Camps, Y. Nicolet), Humana Press, Totowa, NJ, **2014**, pp. 125–137.
- [23] V. Pelmeshnikov, J. A. Birrell, C. C. Pham, N. Mishra, H. Wang, C. Sommer, E. Reijerse, C. P. Richers, K. Tamasaku, Y. Yoda, T. B. Rauchfuss, W. Lubitz, S. P. Cramer, *J. Am. Chem. Soc.* **2017**, *139*, 16894–16902.
- [24] R. Gilbert-Wilson, J. F. Siebel, A. Adamska-Venkatesh, C. C. Pham, E. Reijerse, H. Wang, S. P. Cramer, W. Lubitz, T. B. Rauchfuss, *J. Am. Chem. Soc.* **2015**, *137*, 8998–9005.
- [25] J. Bjerrum, L. G. Sillén, G. K. Schwarzenbach, C. Berecki-Biedermann, *Stability constants of metal-ion complexes, with solubility products of inorganic substances. 2 : Inorganic ligands*, Chemical society, London, **1958**.
- [26] a) K. A. Vincent, J. A. Cracknell, J. R. Clark, M. Ludwig, O. Lenz, B. Friedrich, F. A. Armstrong, *Chem. Commun.* **2006**, 5033–5035; b) V. C. C. Wang, M. Can, E. Pierce, S. W. Ragsdale, F. A. Armstrong, *J. Am. Chem. Soc.* **2013**, *135*, 2198–2206.
- [27] a) D. Sippel, M. Rohde, J. Netzer, C. Trncik, J. Gies, K. Grunau, I. Djurdjevic, L. Decamps, S. L. A. Andrade, O. Einsle, *Science* **2018**, *359*, 1484–1489; b) T. Spatzal, K. A. Perez, O. Einsle, J. B. Howard, D. C. Rees, *Science* **2014**, *345*, 1620–1623.
- [28] M. Razavet, S. J. Borg, S. J. George, S. P. Best, S. A. Fairhurst, C. J. Pickett, *Chem. Commun.* **2002**, 700–701.
- [29] a) Y. Ilina, C. Lorent, S. Katz, J.-H. Jeoung, S. Shima, M. Horch, I. Zebger, H. Dobbek, *Angew. Chem. Int. Ed.* **2019**, *58*, 18710–18714; *Angew. Chem.* **2019**, *131*, 18883–18887; b) E. Siebert, Y. Rippers, S. Frielingsdorf, J. Fritsch, A. Schmidt, J. Kalms, S. Katz, O. Lenz, P. Scheerer, L. Paasche, V. Pelmeshnikov, U. Kuhlmann, M. A. Mroginski, I. Zebger, P. Hildebrandt, *J. Phys. Chem. B* **2015**, *119*, 13785–13796.
- [30] F. M. B. Paulo, T. C. Freire, J. A. Lima, F. E. A. Melo, J. M. Filho, in *Raman Spectroscopy and Applications, Vol. Open access peer-reviewed Edited Volume*, IntechOpen, **2017**.
- [31] K. A. Vincent, A. Parkin, O. Lenz, S. P. J. Albracht, J. C. Fontecilla-Camps, R. Cammack, B. Friedrich, F. A. Armstrong, *J. Am. Chem. Soc.* **2005**, *127*, 18179–18189.
- [32] E. C. Hatchikian, N. Forget, V. M. Fernandez, R. Williams, R. Cammack, *Eur. J. Biochem.* **1992**, *209*, 357–365.

Manuscript received: April 9, 2020

Revised manuscript received: June 1, 2020

Accepted manuscript online: June 2, 2020

Version of record online: July 23, 2020